QUANTITATIVE PETROGRAPHY OF ILMENITE IN LUNAR MARE BASALTS. P. H. Donohue*[1] and C. R. Neal[1], [1]Civil & Environmental Engineering & Earth Sciences, University of Notre Dame, Notre Dame, IN (*pdonohu1@nd.edu; neal.1@nd.edu)

Introduction: Mare volcanism played a significant role in the evolution of the lunar surface and the basaltic samples allow the nature of the lunar interior to be evaluated. However, the basalts returned by Apollo, Luna, and in lunar meteorites may not have remained unmodified since being extracted from their source regions. Thin sections of these basalts are little slices of truth, windows into the complex processes visited upon these igneous rocks. Crystallization processes are reflected in the morphology and size distribution of major phases. High-Ti mare basalts (>6 wt % TiO_2) typically have a mode of ≥10% ilmenite (*c.f.*, [1]). Preliminary quantitative petrographic analysis of ilmenite highlighted the variability of ilmenite textures among A17 high-Ti basalts [2]. Here we show a coupled variation in texture with crystal size distribution (CSD) profile that can be related to experimentally produced textures. We extrapolate these results to show how the A17 high-Ti basalts crystallized in terms of position in a lava flow.

Method: Crystal stratigraphy is a non-destructive technique to quantitatively evaluate rock textures and crystal populations, complemented by *in-situ* mineral analysis. Textural analysis focuses on the use of CSDs to yield a histogram of log-normal population density [*ln(n)*] versus size (*L*) for a given mineral phase. Rather than a traditional histogram, the classic CSD is a line graph connecting the center peaks of size bins and the slope of the resulting CSD profile is a function of growth rate (*G*) and residence time (τ):

$$n = n_0 \exp(-L/G\tau)$$

where n_0 is initial nucleation density [3]. The slope of a CSD is $-1/G\tau$, and is thus linear if nucleation and growth continue uninterrupted during cooling. Non-linear CSDs may result from changes in nucleation rate (e.g., rapid nucleation during eruption), mixed magmas with distinct crystal populations, and other dynamic processes [3-5].

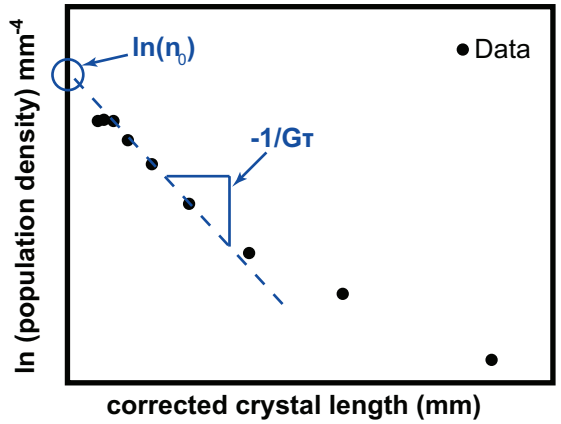

Fig. 1: Anatomy of an CSD, with best-fit line through crystal populations at smaller size bins. Figure adapted from [3].

Ilmenite CSDs have been generated for 19 Apollo 17 high-Ti basalts (four of chemical Type A: 70135, 71048, 74235, 75015; four of Type B1: 70315, 71557, 75075, 78575; five of Type B2: 70275, 71035, 71157, 77516, 79516; four of Type C: 71509, 74255, 74275, 75115; the sole Type D: 79001; and Type U olivine cumulate: 71597), three basalt clast fragments from Apollo 16 breccia 60639, and an Apollo 16 rake sample (60603) classified as a basalt by [6]. Two CSDs were made for 70275, which is dominantly variolitic (label *F* in Fig. 3) but has a coarser subophitic region (label *C*). Textures of these samples range from olivine (micro)-porphyritic (9 of the A17 basalts) and olivine vitrophyric (60603) to plagioclase-poikilitic (9 A17 basalts), allotriomorphic granular (78575), and subophitic (60639).

Thin sections were photomicrographed in reflected light in order to identify ilmenite crystals. High-resolution photomicrographs taken under 5x magnification were mosaiced in *Adobe Photoshop*, allowing crystals ~0.02mm and larger to be identified and traced. The resulting ilmenite crystal traces were measured for length, width and area using an image processing program (*ImageJ* v.1.46, http://rsbweb.nih.gov/ij/). Lengths and widths of the crystal population were compared to a database of 2D intersections of model crystals to obtain a best-fit estimate of original 3D crystal habit (*CSDSlice* v4 [7]). CSD plots were generated by *CSDCorrections* [8], which incorporated the length, width, area, 3D habit, and average roundness of crystals, in addition to sample area measured.

Results: CSD profiles exhibit a range in slope (from linear to concave upward) and maximum extent, reflecting the variety of textures in and processes experienced by the sampled basalts (Fig. 2). While most CSD profiles are subparallel at larger crystal sizes, there is a noticeable fanning out pattern at sizes below ~0.6mm. We focus on crystals in length from 0.02-0.6mm, as all samples have at least three size bins in this range. Additionally, the lower limit of resolution of photomicrographs is ~0.02mm. The slopes and intercepts of CSD profiles in this size range were calculated using size bins for which population density increased with decreasing size (Fig. 3). A decrease in population density at the smallest size bins may indi-

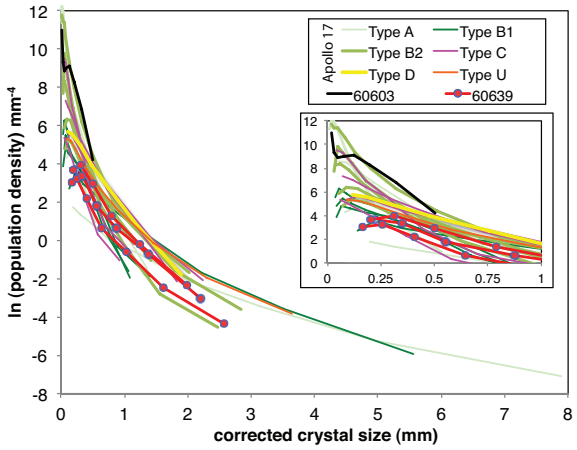

Fig. 2: CSD plots of investigated samples, given as population density versus size. The portion from 0-1mm is inset for clarity.

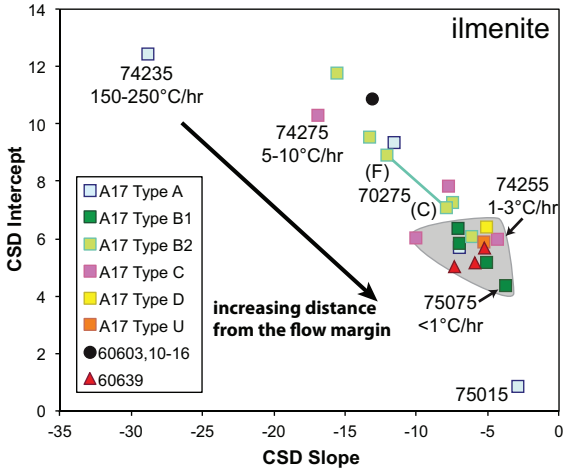

Fig. 3: CSD slope *vs*. intercept for the 0.02-0.6mm range of crystal sizes. The majority of coarse-grained samples plot in the shaded region. Cooling rate estimates from [10].

cate textural coarsening or may be an artifact of the tracing process [9]. These downturns affect the CSD slope and thus size bins with decreasing population density are omitted from calculations.

Discussion: Crystals <0.6mm in length are part of the groundmass, and their morphology and texture indicate the final stage of crystallization occured over a range of cooling rates from <1 to 250°C/hr [10]. Plagioclase-poikilitic basalts (except for 75015) are clustered in Fig. 3 (shaded region). Finer-grained basalts show a larger range in CSD slope (a function of G and τ) and intercept (*e.g.*, nucleation density). Assuming a constant growth rate, ilmenite residence time decreases with increased cooling rates. For experimentally determined growth rates (~3×10^{-7} mm/s for basaltic Fe-Ti oxides [11]), residence times of groundmass ilmenite range from ~1 day (for 74235) to thirteen days (for 75015).

The textural variation in 70275 belies a cooling rate change of up to several degrees at the microscale. At growth rates noted above, residence time varies from 3-5 days. We observe similar but less-extensive clusters of pyroxene-plagioclase intergrowths in some other samples. These may be microcosms of melt that were trapped and insulated to allow for slower cooling.

Quench crystal growth as a result of rapid cooling is reflected in the increasing nucleation density of small crystals, which would be the most readily affected by changes in cooling rate. For the <0.6mm size range investigated, ilmenite crystallization occurred primarily during post-emplacement cooling. Thus the groundmass ilmenite texture and resulting CSD profile is largely a function of location within a lava flow. Overall, groundmass residence times suggests these samples cooled relatively quickly at the surface (*i.e.*, in thin flows) and come from different regions within a given flow (Fig. 3). The Type B1 and B2 basalts in Fig 3 fall along a line, consistent with progressive magma crystallization [12,13]. Textural coarsening could explain the distribution of Type A basalts. Similar comparisons with phenocrysts will aid in building residence times for ilmenite formed prior to eruption.

Future work will incorporate textural studies of ilmenite from Apollo 12 basalts, lunar meteorites and additional Apollo 16 fragments. Comparisons with terrestrial ilmenite studies will determine whether these relationships are consistent between volcanism of the Earth and Moon.

Acknowledgements: This research was supported by NASA grant NNX09AB92G to CRN.

References: [1] Papike J.J., et al. (1976) *Rev. Geophys. Space Phys.* **14**, 475-540. [2] Donohue et al. (2011) LPSC **42**, #2568 (abs). [3] Marsh B. (1988) *Contrib. Mineral. Petrol.* **99**, 277-291. [4] Cashman K. and Marsh B. (1988) *Contrib. Mineral. Petrol.* **99**, 292-305. [5] Marsh B. (1998) *J. Petrol.* **39**, 553-599. [6] Zeigler, R.A. *et al.* (2006) *MaPS* **41**, 263-284. [7] Morgan D. J. and Jerram D. A. (2006) *J. Volc. Geotherm. Res.* **154**, 1-7. [8] Higgins M. D. (2000) *Am. Min.* **85**, 1105-1116. [9] Higgins M. D. (1996) *J. Volc. Geotherm. Res.* **70**, 37-48. [10] Usselman T. M. et al. (1975) *Proc. Lunar Sci. Conf.* ***6th***, 997-1020. [11] Burkhard, D. J. M. (2005) *Eur. J. Mineral.* **17**, 675-685. [12] Zieg M. J. and Marsh B. (2002) *J. Pet.* **43**, 85-101. [13] Zieg M. J. and Lofgren G. (2006) *J. Volc. Geotherm. Res.* **154**, 74-88.